Journal of Drug Delivery Science and Technology 114 (2025) 107392

Contents lists available at ScienceDirect

Journal of Drug Delivery Science and Technology

journal homepage: www.elsevier.com/locate/jddst

Battery-free, sprayable, wireless photothermal micro/nanofibre dressing with thermal-induced crosslinked polypyrrole for accelerated diabetic wound healing

Chun-Chi Chang [a,1], Ting-Chiau Huang [b,1], Jia-Wei Liang [c], Sih-Chi Chuang [d,e], Ching-Cheng Huang [b], Hieu Trung Nguyen [f], Hsien-Tsung Lu [g,h,i,*], Ke-Hung Tsui [j,k,**], Andrew E.-Y. Chuang [c,l,***]

[a] Department of Biotechnology and Pharmaceutical Technology, Yuanpei University of Medical Technology, Hsinchu, Taiwan
[b] Department of Biomedical Engineering, Ming-Chuan University, Taoyuan city, Taiwan
[c] Graduate Institute of Biomedical Materials and Tissue Engineering, College of Biomedical Engineering, Taipei Medical University, New Taipei City, Taiwan
[d] Department of Chemical Engineering and Biotechnology, National Taipei University of Technology, Taipei, 10608, Taiwan
[e] Doctoral Program of Biochemical and Biomedical Engineering, National Taipei University of Technology, Taipei, 10608, Taiwan
[f] Department of Orthopedics and Trauma, Faculty of Medicine, University of Medicine and Pharmacy at Ho Chi Minh City, Ho Chi Minh City, 700000, Viet Nam
[g] Department of Orthopedics, School of Medicine, College of Medicine, Taipei Medical University, Taipei, 11031, Taiwan
[h] International Ph.D. Program in Cell Therapy and Regenerative Medicine, College of Medicine, Taipei Medical University, Taipei, 11031, Taiwan
[i] Department of Orthopedic, Taipei Medical University Hospital, Taipei City, 11031, Taiwan
[j] Department of Urology, Shuang Ho Hospital, Taipei Medical University, Taipei, 110, Taiwan
[k] Department of Urology, School of Medicine, College of Medical, Taipei Medical University, Taipei, 110, Taiwan
[l] Cell Physiology and Molecular Image Research Center, Taipei Medical University-Wan Fang Hospital, Taipei, 11696, Taiwan

ARTICLE INFO

Keywords:
Wearable phototherapy
Diabetic wound healing
Near-infrared (NIR) light
Photothermal bandage
Electrospun nanofibers
Smart dressing

ABSTRACT

Diabetic chronic wounds remain a formidable clinical challenge because hyperglycaemia triggers microangiopathy, persistent inflammation, and oxidative stress that disrupt the orderly cascade of tissue repair. Near-infrared (NIR) phototherapy offers a wireless, non-invasive, electromagnetic approach that has shown clinical success, yet conventional devices are typically bulky, expensive, and require prolonged treatment times factors that hamper patient adherence and therapeutic efficacy. To address these limitations, we developed a lightweight, sprayable, wearable phototherapeutic system that couples a flexible, battery-free bandage with a portable NIR light source. The bandage is an ultra-flexible electrospun micro/nanofibre membrane composed of sodium-chloride–templated polypyrrole, polyethyleneimine, and PLGA; it converts incident NIR energy into heat and delivers it directly to the wound site.

Electromagnetic simulations and empirical measurements confirm that the spray-deposited bandage generates a homogeneous photothermal field suitable for wound therapy. Under 808 nm irradiation, the membrane rapidly reaches around 45 °C within 3 min and withstands repeated on/off cycles without performance loss. This mild hyperthermia up-regulates heat-shock proteins and mitigates reactive oxygen species. In vitro, the membrane supports L929 fibroblast proliferation and exhibits negligible cytotoxicity at extract concentrations up to 30 %. In streptozotocin-induced diabetic Wistar rats, a single application of the bandage followed by daily 5-min NIR illumination accelerates wound closure by day 7, compared with untreated controls, and is accompanied by potentially reduced inflammatory pathogenic substance infiltrates. Collectively, these results demonstrate that integrating conductive and photothermal cues within a wearable scaffold offers a simple yet powerful strategy to overcome the multifactorial barriers of diabetic wound healing and underscores the translational promise of this intelligent, light-responsive dressing.

* Corresponding author. Department of Orthopedics, School of Medicine, College of Medicine, Taipei Medical University, Taipei, 11031, Taiwan.
** Corresponding author. Department of Urology, School of Medicine, College of Medical, Taipei Medical University, Taipei, 110, Taiwan.
*** Corresponding author. Graduate Institute of Biomedical Materials and Tissue Engineering, College of Biomedical Engineering, Taipei Medical University, New Taipei City, Taiwan.
E-mail addresses: lu7788@tmu.edu.tw (H.-T. Lu), t2130@s.tmu.edu.tw (K.-H. Tsui), eychuang@tmu.edu.tw (A.E.-Y. Chuang).
[1] These authors contributed equally.

https://doi.org/10.1016/j.jddst.2025.107392
Received 13 April 2025; Received in revised form 7 August 2025; Accepted 10 August 2025
Available online 13 August 2025
1773-2247/© 2025 Published by Elsevier B.V.

1. Introduction

Diabetic foot ulcers represent one of the most challenging and persistent skin-related complications associated with diabetes mellitus. Every year, approximately 18.6 million individuals across the globe will experience at least one occurrence of these painful ulcers [1,2]. The lifetime risk of developing a foot ulcer for those living with diabetes has now escalated to nearly one in three. This alarming statistic underscores the severity of the condition. The pathophysiology of diabetic foot ulcers is multifactorial, primarily driven by hyperglycemia, which leads to microangiopathy and neuropathy [3]. These conditions trigger a persistent state of inflammation and oxidative stress, disrupting the finely-tuned processes involved in wound healing. Under normal circumstances, wound repair involves a well-orchestrated sequence of hemostasis, inflammation, proliferation, and remodeling. In diabetic patients, however, this cascade is derailed, leading to significant healing challenges [4–6]. Traditional wound dressings typically provide a barrier to protect the wound and maintain moisture; however, they fall short in addressing critical underlying issues. These dressings do not alleviate tissue hypoxia, which is a lack of oxygen in the wound area, nor do they effectively manage chronic infections or improve the altered oxidative environment that is characteristic of diabetic wounds. As a result, the median healing time for these ulcers can span over five months. Alarmingly, large percentage ulcers that fail to heal can lead to lower-limb amputation, and the five-year mortality rate for these patients is comparable to that of many aggressive cancers. This stark reality emphasizes the urgent need for better therapeutic strategies and wound management practices tailored specifically to the unique challenges posed by diabetic foot ulcers (see Scheme 1).

Near-infrared (NIR) phototherapy has become a promising approach in modern medicine, functioning as a wireless and non-invasive method to induce localized hyperthermia [7]. This therapeutic technique enhances blood circulation, boosts the production of heat-shock proteins, and displays a range of antibacterial properties that can combat infections effectively [8]. While there have been attempts to reduce the size of the light sources used in these therapies, the crucial element known as the therapeutic interface the dressing that facilitates the transfer of optical energy into the wound has not seen significant advancements in engineering. This inadequacy poses a barrier to fully realizing the potential benefits of NIR phototherapy, as an effective dressing is essential for ensuring optimal energy delivery and patient comfort during treatment sessions. In recent studies it's reported that applying mild hyperthermia to tumors helped loosen their dense structure and improve blood perfusion within the tumor. Additionally, compared to high-temperature hyperthermia (>50 °C), mild hyperthermia (43°C-46 °C) appears more effective in stimulating the immune system [9,10]. Electrospinning presents an innovative method for producing micro- and nanofiber membranes that closely resemble the native extracellular matrix (ECM) [11]. This architectural similarity plays a crucial role in facilitating essential biological processes such as gas exchange, the management of exudates, and promoting intimate contact with tissues. Recent research indicates that near-infrared (NIR)-responsive electrospun dressings are capable of effectively eliminating biofilms in a matter of minutes at elevated temperatures of 52 °C. Moreover, when these materials are applied at lower temperatures, specifically around 42 °C, they can enhance fibroblast migration, encourage angiogenesis, and potentially exert beneficial effects on tissue regeneration [12].

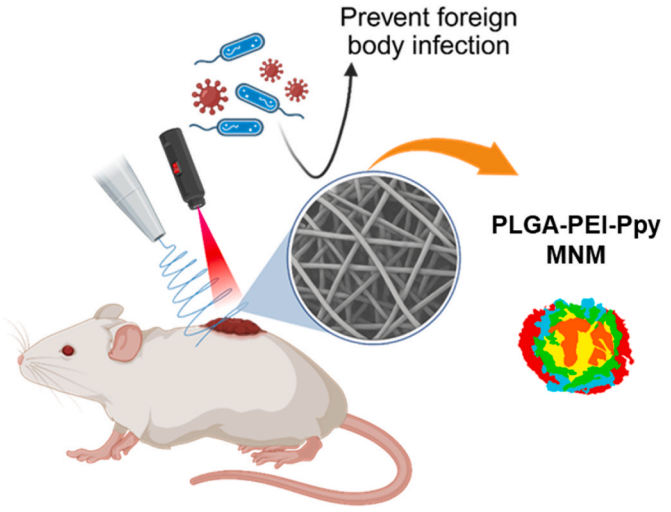

Scheme 1. Conceptual roadmap of the study. A multifunctional sprayable and wearable electrospun membrane (PLGA–PEI–PPy MNM) was developed by embedding sodium chloride–templated polypyrrole (PPy) within a PLGA matrix and complexing it with PEI, forming a flexible, conductive, and photothermally responsive micro/nanofibrous network. In a streptozotocin-induced diabetic Wistar rat model with full-thickness dorsal wounds, the membrane was spray-applied, worn as a bandage, and exposed to daily NIR irradiation, resulting in accelerated wound healing. Illustration created using BioRender.

Near-infrared (NIR)-responsive electrospun dressings have emerged as a promising therapeutic strategy for infected wound healing, especially in diabetic environments characterized by persistent infection and delayed tissue regeneration. These smart dressings leverage the photothermal conversion capability of nanomaterials to produce localized heating upon NIR irradiation, enabling dual-action benefits—rapid bacterial eradication through high-temperature sterilization and promotion of tissue repair through mild hyperthermia. For instance, MXene-loaded microgel nanofiber membranes have demonstrated programmable photothermal therapy (PPT) and mild photothermal therapy (MPTT), achieving broad-spectrum antibacterial effects within minutes and enhancing fibroblast proliferation and neovascularization under controlled temperatures. Similarly, botanicals-based nanofibrous membranes integrating tannic acid–Fe(III) nanoparticles and berberine hydrochloride provide synergistic antibacterial activity and accelerated wound closure through heat-triggered drug release. These NIR-responsive dressings are highly porous, hydrophilic, breathable, and biocompatible, offering a multifunctional platform that not only combats biofilm-associated infections but also supports tissue regeneration. Recent advancements in such NIR-responsive electrospun systems underscore their translational potential in addressing the multifaceted challenges of infected and chronic wounds [13–15].

Among the various materials investigated for these applications, polypyrrole (PPy), a π-conjugated conductive polymer stands out due to its remarkable ability to convert NIR light into heat with high efficiency. This property not only allows for precise thermal stimulation but also provides an electrical pathway that can emulate the endogenous bioelectric signals crucial for effective wound healing. Despite its advantageous characteristics, PPy in its pure form exhibits brittleness which poses challenges for processing it into flexible, free-standing mats. To address these limitations, blending PPy with poly (lactic-co-glycolic acid) (PLGA), a biodegradable copolymer that is widely recognized and approved for clinical use, enhances the mechanical strength and durability of the resulting material. This blend improves structural integrity while maintaining the desired functionalities. Furthermore, incorporating polyethyleneimine (PEI) into the composite not only aids in achieving a homogeneous dispersion of PPy within the matrix but also imparts a positively charged surface that fosters cell adhesion, thereby creating a more conducive environment for tissue interaction and healing [16].

Building upon our previous findings, we propose a novel, spray-deployable, ultra-flexible micro/nanofibre membrane that incorporates a sodium chloride (NaCl)-templated composite of PPy, PEI, and PLGA. This innovative membrane is designed to work in conjunction with a lightweight NIR emitter, delivering synchronized photothermal and conductive stimulation directly to the diabetic wound bed,

ultimately enhancing the tissue repair process. NaCl was used as background electrolyte and potential stabilizer in the aqueous system [17]. Unlike previously developed photothermal membranes, which depend on cumbersome wired laser systems or heavy battery packs, our design is entirely battery-free. It is engineered to adhere closely to the complex contours of irregular skin surfaces, allowing for a customized and convenient at-home therapy experience for patients.

Lei et al. reported a hyaluronic acid-based microneedle platform functionalized with biomineralized melanin nanoparticles for combined photothermal tumor therapy and tissue regeneration. This reference supports the dual application potential of PTT platforms [18]. Apart from thatsome studies provides a comprehensive review on intelligent hydrogels with multifunctional properties such as injectability, self-healing, shape-memory, and responsiveness that synergistically promote diabetic wound healing through antibacterial, antioxidant, and immunomodulatory mechanisms [19]. Xu et al. which presents a multifunctional hydrogel incorporating gelatin methacrylate (GelMA), Bletilla Striata polysaccharide, and TA/Fe^{3+} complexes, demonstrating immunomodulatory effects by inducing M2 macrophage polarization, promoting angiogenesis, and accelerating diabetic wound closure [20].

To validate the approach, researchers conducted finite-element electromagnetic simulations alongside experimental thermography assessments. These investigations demonstrated that our membrane generates a spatially uniform photothermal field, achieving therapeutic temperatures indicative of mild hyperthermia within just 3 min when exposed to 808 nm light [21]. Researchers further hypothesize that this controlled, transient hyperthermic treatment will effectively up-regulate the expression of heat-shock proteins, reduce levels of reactive oxygen species, and, when combined with the conductive network of the membrane, promote critical biological processes such as fibroblast proliferation, neovascularization, and skin remodeling [22]. Collectively, these mechanisms are expected to facilitate wound healing and regeneration, thus addressing a pressing need in the management of diabetic wounds.

The current investigation is designed to accomplish three distinct objectives, as plotted in **Sch. 1**. Firstly, we aim to synthesize and comprehensively characterize a sophisticated micro/nanofibre membrane composed of thermally polymerized PPy, PEI, and PLGA upon NaCl aqueous phase (PLGA PEI PPy micro/nanofibre membrane (PLGA-PEI-PPy MNM)), specifically tailored to exhibit enhanced functionality and superior photothermal properties [23]. Secondly, we plan to assess the cytocompatibility of this innovative membrane/matrix while also exploring its mechanistic effects on oxidative stress levels, reduced inflammatory cytokine, avoided the potential pathogenic substance, and the expression of heat-shock proteins. This evaluation will provide insights into the membrane's interaction with cellular environments under various stress conditions [24]. Lastly, we investigate the therapeutic efficacy of the developed membrane in a preclinically relevant animal model specifically, a streptozotocin-induced diabetic rat model featuring full-thickness wounds [25]. This assessment would be conducted under a controlled regimen of near-infrared (NIR) irradiation applied daily for brief periods. By addressing these critical gaps in existing knowledge particularly concerning the integration of effective photothermal conversion, enhanced electrical conductivity, and user-friendly conformal fit into a single, multifunctional wound dressing we aspire to deliver a clinically applicable solution. This solution is intended to overcome the complex barriers associated with diabetic wound healing and pave the way for the development of next-generation intelligent bandages that can improve patient outcomes.

2. Experimental section

2.1. Materials

Pyrrole, with a purity of 98 %, was sourced from Sigma-Aldrich, alongside branched polyethyleneimine, characterized by a molecular weight of 25 kDa, and PLGA in a 50:50 ratio, exhibiting an intrinsic viscosity of 0.8 dL g^{-1}. Additionally, reagents such as sodium chloride, hydrochloric acid, and sodium hydroxide were procured from Merck and integrated into the experiments without any further modifications.

For the biological component of the study, L929 mouse fibroblasts were obtained from the reputable BCRC cell bank, ensuring the validity and reliability of the cellular models used. Male Wistar rats, each weighing between 250 and 300 g, were provided by BioLasco (Taipei, Taiwan) and they were managed at TMU Laboratory Animal Centre. Importantly, all experimental procedures involving these animals were rigorously reviewed and sanctioned by the Institutional Animal Care and Use Committee, under the approval number (SHLAC2025-0051), ensuring compliance with ethical standards in animal research.

2.2. Synthesis of PEI-PPy complex

A precise quantity of 0.3 g and PEI (0.3 g) was carefully dissolved in 50 mL of 95 % ethanol, which had been supplemented with 0.2 M NaCl under consistent magnetic stirring to ensure complete homogenization. Oxidative polymerization was conducted in an 80 °C oven, with the solution pH carefully adjusted to either 0.8 or 7.0 by the gradual addition of hydrochloric acid (HCl) or 1 M sodium hydroxide (NaOH), respectively. To remove any unreacted materials and impurities, the mixture was subjected to dialysis against deionized water for a period of 48 h. This process resulted in the successful synthesis of the PEI-PPy (NaCl) complex, characterized by its stable dispersion and enhanced properties due to the interaction between the components.

2.3. Fabrication of PLGA-PEI-PPy micro/nanofibre membrane (PLGA-PEI-PPy MNM)

PLGA and PEI doped with PPy (PLGA-PEI-PPy MNM) were meticulously co-dissolved in hexafluoro-2-propanol, achieving a spinning solution with a concentration of 12 % (w/v) at a weight ratio of 9:1. The electrospinning process was conducted utilizing a 21-gauge stainless-steel needle, applying a high voltage of 18 kV to facilitate the formation of micro/nanofibers (See the **Supplementary Video**). The device was obtained from Siward Crystal Technology Co., Ltd. (Taichung City, Taiwan). The feed rate was carefully set to 0.8 mL per hour, and the distance between the needle tip and collector was maintained at 15 cm to ensure effective fiber alignment and deposition. Once the electrospinning was complete, the resulting nanofiber mat was subjected to a vacuum drying process overnight to remove any residual solvents. Finally, the dried mat was meticulously cut into circular dressings with a diameter of 20 mm, preparing them for potential applications in wound healing and tissue engineering.

2.4. Characterization

The morphology of the samples was meticulously investigated using scanning electron microscopy (SEM), specifically with the Hitachi model SU3500, allowing for detailed visualization of surface structures. To quantify the fibre diameter accurately, ImageJ software was employed, providing precise measurements critical for assessing material properties. The elemental distribution within the samples was analyzed using energy-dispersive X-ray spectroscopy (EDX), which facilitated a comprehensive understanding of the elemental composition.

To confirm the chemical structure and crystallinity of the materials under study, Fourier-transform infrared spectroscopy (FTIR) was conducted with the Nicolet iS50 instrument, alongside X-ray diffraction (XRD) analysis utilizing the Bruker D8, ensuring a thorough characterization of the materials' structural attributes. The hydrophilicity of the samples was evaluated through static water contact angle measurements, using the Krüss DSA30, which provided insights into the surface wettability and potential applications. In addition, dynamic light scattering (DLS) measurements were performed with the Malvern Zetasizer

Nano ZS to ascertain the particle size of the spinning precursor, giving valuable data on the dispersion characteristics of the materials.

Electrical conductivity was quantified using a four-point probe method with the Keithley 2400, which delivers accurate resistance measurements critical for electronic applications. Furthermore, the photothermal performance of the materials was assessed by subjecting 1 cm^2 membrane discs to an 808 nm laser (with an intensity of 2 W/cm^2 and a spot diameter of 6 mm) while immersed in 1 mL of phosphate-buffered saline (PBS). Temperature readings were meticulously recorded using an infrared camera (A-BF RX300) and a thermocouple (Lutron TM-925), providing detailed insights into the thermal behavior of the membranes under irradiation.

2.5. In vitro cytocompatibility

To prepare the extracts, 100 mg of membrane material was incubated in 10 mL of Dulbecco's Modified Eagle Medium (DMEM) at a controlled temperature of 37 °C for a duration of 12 h. This incubation step was followed by filtration through 0.22 μm membranes to obtain a clarified extract. Subsequently, L929 cells were carefully seeded into 96-well plates at a density of 2×10^4 cells per well. After a growth period of 24 h to allow the cells to adhere and proliferate, the medium was replaced with varying concentrations of the prepared extracts, specifically at 10 %, 30 %, and 100 % (v/v). Following another 24-h incubation period with the extracts, the assessment of cell viability was conducted using the MTT assay. For this assay, a solution of 0.5 mg/mL of MTT was introduced to each well and incubated for 4 h. After this incubation, the absorbance was measured at a wavelength of 570 nm to quantify the viability of the cells based on their metabolic activity.

2.6. Diabetic wound model and in vivo experiments

Diabetes was induced in the rats through a precise protocol involving a single intraperitoneal injection of streptozotocin at a dosage of 65 mg/kg, diluted in a 0.1 M citrate buffer with a pH of 4.5. After a one-week monitoring period, only those rats exhibiting fasting blood glucose levels exceeding 16.7 mmol/L were selected for the study. To initiate the wound healing experiment, the rats were placed under isoflurane anesthesia for a humane surgical procedure. Carefully, the dorsal fur was shaved to ensure a clean surface and two symmetrical circular wounds were created on the back of each rat. These wounds, measuring around 20 mm in diameter, were made using a sterile biopsy punch, ensuring consistent wound size across subjects.

The rats were then randomly assigned to one of three experimental groups, each consisting of six wounds: a control group that received no dressing, a group treated with a PLGA combined with NIR light therapy, and a group that received a dressing modified with PLGA-PEI-PPy MNM alongside NIR therapy. After which the wounds were subjected to irradiation with an 808 nm laser at a power density of 2 W/cm^2 for a duration of 5 min each day. Throughout the experimental period, the wound area was meticulously monitored and documented. Photographic images of the wounds were captured on specified days 0, 1, 3, 5, and 7 allowing for detailed analysis and quantification of wound healing via ImageJ software.

Fluorescence imaging was conducted using an IVIS Spectrum system, utilizing FITC-labeled membranes and Cy5-conjugated lipopolysaccharide (LPS) to assess the penetration, interaction, and distribution of the applied treatments within the wound sites. This comprehensive approach ensured a thorough investigation of the efficacy of the different dressings in enhancing wound healing in diabetic rats.

On the seventh day following the initial procedure, the rats were humanely euthanized to collect wound tissues and major organs for further analysis. Histological examination was performed utilizing Hematoxylin and Eosin (H&E) staining as well as Masson's trichrome staining to assess tissue structure and healing. Additionally, immunohistochemistry techniques were employed to evaluate the expression of specific biomarkers, including CD31 (indicative of angiogenesis), and HSP70 (a stress response protein).

2.7. Statistical analysis

Data were represented as the average value accompanied by the standard deviation (SD) to indicate the variability around the mean. Statistical Analysis was done using GraphPad Prism software. The One-Way ANOVA was employed to assess statistical significance, with significance level denoted as follows. *p(0.05), **p(0.01),***p(0.001) and ****p(0.0001). A significance level of $P < 0.05$ was established, indicating that any observed differences would be considered statistically meaningful and not likely due to random chance.

2.8. Physicochemical characterization of PLGA-PEI-PPy MNM

2.8.1. Redox behavior and polymerization confirmation

To assess the redox environment during the synthesis process, oxidation–reduction potential (ORP) measurements (Fig. 1A) were conducted before and after pyrrole polymerization within the polyethyleneimine (PEI)-stabilized system. Prior to polymerization, the pyrrole/PEI precursor mixture exhibited relatively low ORP values (~150 mV), indicating a weakly oxidative environment. However, following thermal polymerization at 80 °C in the presence of NaCl, an increase in ORP (~320 mV) was observed in the PEI-PPy complex, confirming the formation of a more oxidizing, electron-deficient conductive matrix. This increase reflects the oxidation of pyrrole into polypyrrole and the emergence of a redox-active framework, further stabilized by the ionic strength provided by NaCl as a background electrolyte. These findings reinforce the role of NaCl not only in templating the network but also in promoting homogeneity and stability of the redox-active polymer dispersion.

2.8.2. Zeta potential and colloidal stability

Zeta potential measurements were performed to probe the surface charge characteristics of individual components and the final composite membrane. Ethanol and PLGA exhibited near-neutral zeta potentials (−1.4 mV and −2.5 mV, respectively)., Pyrrole (Py) and PEI-PPy complexes displayed intermediate potentials (~+2.8 mV and +3.5 mV), suggesting partial surface charge masking due to polymerization (Fig. 1B). Interestingly, the electrospun PLGA-PEI-PPy MNM revealed a modestly negative surface potential (−5.3 mV), indicative of PLGA surface dominance post-electrospinning and suggesting a stabilized, slightly anionic surface profile. This moderate zeta potential is conducive to dispersion stability and cellular interaction, making the formulation ideal for subsequent biological applications.

2.8.3. Wettability and surface energy

The water contact angle analysis (Fig. 1C) revealed critical insights into the wettability of the materials. The native PLGA exhibited a highly hydrophobic profile with a contact angle, reflecting poor water affinity. In contrast, normal (water) substrates (as a reference) demonstrated a lower angle of ~38°, confirming their hydrophilic nature. Notably, the PLGA-PEI-PPy MNM displayed an intermediate contact angle, indicating that the introduction of PEI and PPy into the PLGA matrix conferred a moderate increase in hydrophilicity. This result is particularly promising, as moderately hydrophilic surfaces are known to support cell adhesion and nutrient diffusion, thereby enhancing the biological functionality of the membrane for wound healing applications.

2.8.4. FTIR Spectral analysis and chemical confirmation

FTIR spectra (Fig. 1D) were employed to elucidate the functional group interactions and confirm the chemical composition of the individual and composite materials. For PLGA (blue spectrum), characteristic C=O stretching (~1750 cm^{-1}) and C–O stretching (~1180 cm^{-1}) were observed. NaCl, used as a dispersant, presented a flat baseline

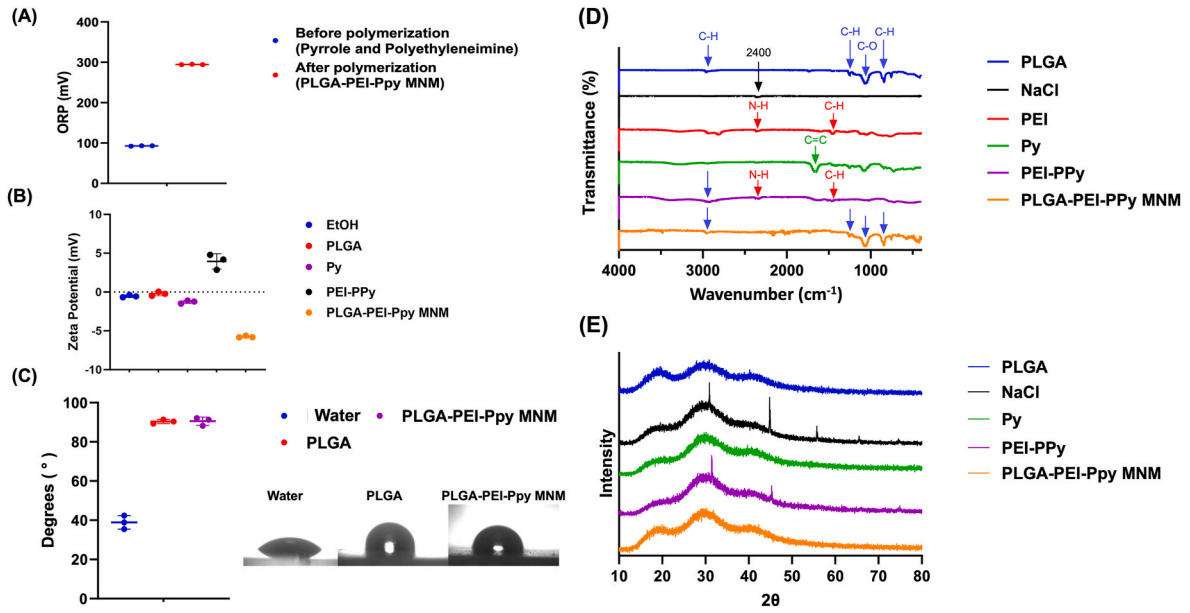

Fig. 1. Physicochemical characterization of the PLGA-PEI-PPy micro/nanofibre membrane (PLGA-PEI-PPy MNM). (A) ORP measurements showed an increase after polymerization, confirming redox-active PEI–PPy complex formation. (B) Zeta potential analysis revealed surface charge modulation across components, with final PLGA–PEI–PPy MNM exhibiting a balanced profile. (C) Water contact angle testing showed enhanced hydrophilicity of the PLGA-PEI-PPy MNM compared to pure PLGA. (D) FTIR spectra confirmed successful integration of all components via characteristic functional group peaks. (E) XRD patterns showed reduced crystallinity in the final PLGA-PEI-PPy MNM, indicating improved flexibility suitable for wearable wound dressings.

without characteristic peaks, confirming its inert infrared profile. PEI (red) exhibited distinct N–H bending (~1570 cm^{-1}) and C–H stretching (~2930 cm^{-1}), while pyrrole (green) revealed vibrational modes associated with C=C and C–H in-plane bending (~1540 cm^{-1} and ~1460 cm^{-1}, respectively). Post-polymerization, the PEI-PPy complex (purple) demonstrated merged features from both PEI and pyrrole, indicating successful chemical integration. The final PLGA-PEI-PPy MNM (orange) retained key peaks from PLGA and PEI-PPy, including shifts in the C–H and N–H regions, suggesting strong electrostatic and possibly hydrogen bonding interactions among components. This corroborates the successful synthesis of a chemically hybridized and compositionally stable micro/nanofibre network.

2.8.5. X-ray diffraction and crystallinity profile

XRD analysis (Fig. 1E) provided further structural insights into the composite material's crystallinity. Pure PLGA exhibited a broad amorphous hump centered around 18°, consistent with its semicrystalline nature. PEI-PPy complexes displayed diffused peaks, indicating a lower degree of order, typical for conductive polymers. Pyrrole (green) showed weak crystallinity signatures, while NaCl exhibited sharp crystalline peaks, as expected from its ionic lattice. Notably, the final PLGA-PEI-PPy MNM displayed a broadened, low-intensity diffraction profile, suggesting a predominantly amorphous structure. This transition toward amorphization is beneficial for mechanical flexibility and surface conformity—key attributes for skin-conformal bandages. The loss of long-range crystalline order also implies effective polymer blending and integration, which further validates the electrospinning and thermal polymerization processes employed.

Together, the ORP elevation, optimized zeta potential, moderate wettability, distinct FTIR signatures, and amorphous XRD profile confirm the successful fabrication of a multifunctional, homogeneous, and photothermally responsive PLGA-PEI-PPy MNM. These properties are fundamental for the subsequent biological and in vivo performance, especially in the context of photothermal stimulation, tissue integration, and reactive oxygen species modulation in diabetic wound environments.

2.9. Elemental composition and microstructural mapping of electrospun membranes

To elucidate the spatial distribution and elemental integration of the fabricated fibrous membranes, energy-dispersive X-ray spectroscopy (EDS) mapping combined with scanning electron microscopy (SEM) was employed. As illustrated in Fig. 2, comparative elemental analysis was conducted on the pristine PLGA electrospun membrane and the composite PLGA-PEI-PPy micro/nanofibre membrane (PLGA-PEI-PPy MNM). The SEM micrographs demonstrate that while both materials exhibit uniform fibrous morphologies, the PLGA-PEI-PPy MNM displays a more intricate surface architecture with intensified topographical undulations, implying the incorporation of electroactive PPy chains and PEI complexes during electrospinning.

The EDS spectrum of the pristine PLGA sample reveals a matrix predominantly composed of carbon and oxygen, consistent with the polymer's backbone. The carbon content reaches 69.2 % by mass (54.5 % atomically), and oxygen contributes 41.7 % by normalized mass, forming a clean and oxygen-rich profile. Nitrogen is detected in trace amounts (1.89 % atomically), likely residual from solvents or minor contaminants, whereas other elements such as fluorine and chlorine appear at negligible levels. Notably, sodium and silicon are nearly undetectable, reaffirming the chemical purity of the base polymer matrix.

In contrast, the PLGA-PEI-PPy MNM shows a distinct elemental profile characterized by an increased nitrogen signal and reduced oxygen-to-carbon ratio. The nitrogen content rises to 2.17 % (atomic), indicative of successful integration of PEI and thermally polymerized polypyrrole, both of which contain abundant amino or imine groups. Meanwhile, carbon content changes to 55 % and oxygen to 33.9 % by normalized mass, highlighting a shift in molecular composition that aligns with the introduction of conductive, non-oxygenated aromatic heterocycles. The composite also shows a slight but definitive presence of sodium (0.21 % atomically), attributed to residual NaCl used during polymerization, which served as an electrochemical template and dispersant. This supports the hypothesis that NaCl not only stabilized the PPy polymerization process in aqueous ethanol but also subtly modified the ionic environment of the final membrane without compromising

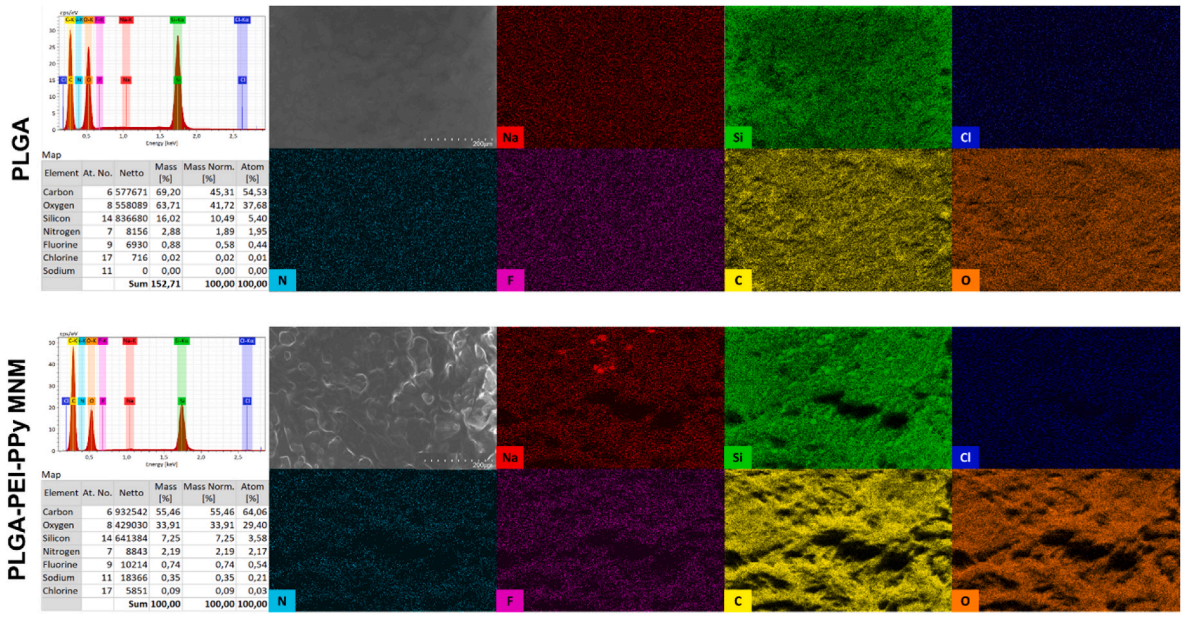

Fig. 2. SEM-EDS elemental mapping of electrospun membranes. Representative SEM and EDS analysis of pristine PLGA and composite PLGA–PEI–PPy MNM membranes. EDS spectra confirm successful incorporation of nitrogen-rich PEI and polypyrrole, with increased nitrogen and residual sodium in the PLGA-PEI-PPy MNM. Elemental mapping shows uniform distribution of C, O, N, F, Cl, Si, and Na throughout the fibrous network, validating the membrane's structural integrity and compositional uniformity.

material uniformity.

Elemental mapping further corroborates the compositional transitions. The carbon and oxygen signals in both membranes are distributed homogeneously, confirming uniform fiber formation. In the PLGA-PEI-PPy MNM, nitrogen mapping exhibits widespread presence throughout the membrane surface, revealing a consistent integration of PEI and PPy throughout the fiber network. The presence of silicon and fluorine in both samples appears minimally variable and likely results from atmospheric deposition or minor instrumental artifacts. Meanwhile, sodium localization in the composite sample appears constrained and sparse, reinforcing the notion of effective but minimal ionic retention post-synthesis. Chlorine, detectable at comparable levels across both membranes, reflects either remnant HCl from pH adjustment or residual salt by-products, with no evident clustering or phase separation.

Overall, the EDS results highlight a distinct chemical transition from a simple biodegradable matrix to a complex, multifunctional electroactive scaffold. The chaned nitrogen signature, along with the emergence of sodium and modified C/O ratios, provides compelling evidence of successful molecular integration and interfacial hybridization within the PLGA-PEI-PPy MNM. Furthermore, the spatial homogeneity observed in elemental distributions supports the processing reproducibility of the electrospinning method and underscores the material's readiness for subsequent photothermal and biological performance evaluations.

2.10. Morphological examination and NIR-triggered photothermal response of electrospun membranes

To investigate the morphological integrity of the electrospun membranes prior to photothermal testing, bright-field optical microscopy was employed. As presented in Fig. 3A, images A1 through A3 correspond to the same PLGA-only sample observed under progressively increasing magnification, while images B1 through B3 represent the PLGA-PEI-PPy MNM under analogous optical settings. These sequential image sets are derived from identical membrane groups but captured at distinct spatial resolutions to provide a layered view of fibrous architecture across multiple scales. This approach allows for a systematic comparison of structural homogeneity, fiber density, and particulate inclusions, thereby eliminating the possibility of misinterpretation as image duplication or improper data reuse.

The PLGA membrane (A1–A3) exhibited a consistent network of randomly oriented micro/nanofibres, free of visible aggregates or compositional discontinuities. At higher magnifications (A3), the individual fiber strands appeared smooth, continuous, and uniform in diameter, affirming the morphological regularity of the unmodified polymer system. In contrast, the PLGA-PEI-PPy MNM (B1–B3) showed a orgnized fiber distribution interspersed with dark granules that became more prominent under increased magnification (B3). These inclusions are presumed to be polypyrrole-rich domains, either embedded within or adhered to the fiber surface, a consequence of the in situ polymerization process during formulation. Importantly, despite this heterogeneity, the overall fibrous structure remained intact and well-distributed, supporting the mechanical and process compatibility of PPy and PEI incorporation.

The photothermal performance of the samples was then evaluated under NIR stimulation using a laser source (808 nm, 2 W/cm^2), with results shown in Fig. 3B. Thermographic imaging after a 5-min irradiation period revealed a substantial difference in thermal response between PLGA and PLGA-PEI-PPy MNM membranes. PLGA alone exhibited only a modest increase in surface temperature ($\Delta T \approx$ 6.47–6.87 °C), reflecting its intrinsic optical transparency and poor NIR absorbance. Conversely, the composite PLGA-PEI-PPy MNM demonstrated robust photothermal conversion, reaching a temperature elevation of up to $\Delta T \approx 14$ °C under identical conditions. This elevated heat output is attributable to the π-conjugated structure of polypyrrole, which effectively absorbs NIR light and dissipates it as localized heat. Additionally, the uniform distribution of PEI may have facilitated homogeneous PPy dispersion during electrospinning, thereby optimizing the thermal field. Time-resolved temperature profiles further delineate these differences, with temperature curves plotted as a function of irradiation time (lower panel, Fig. 3B). While PLGA and Py groups displayed only minimal thermal accumulation, the PLGA-PEI-PPy MNM group demonstrated a rapid and linear increase in temperature. This threshold falls within the mild hyperthermia range known to activate heat-shock protein expression without causing thermal damage, supporting the therapeutic relevance of this photothermal system. In

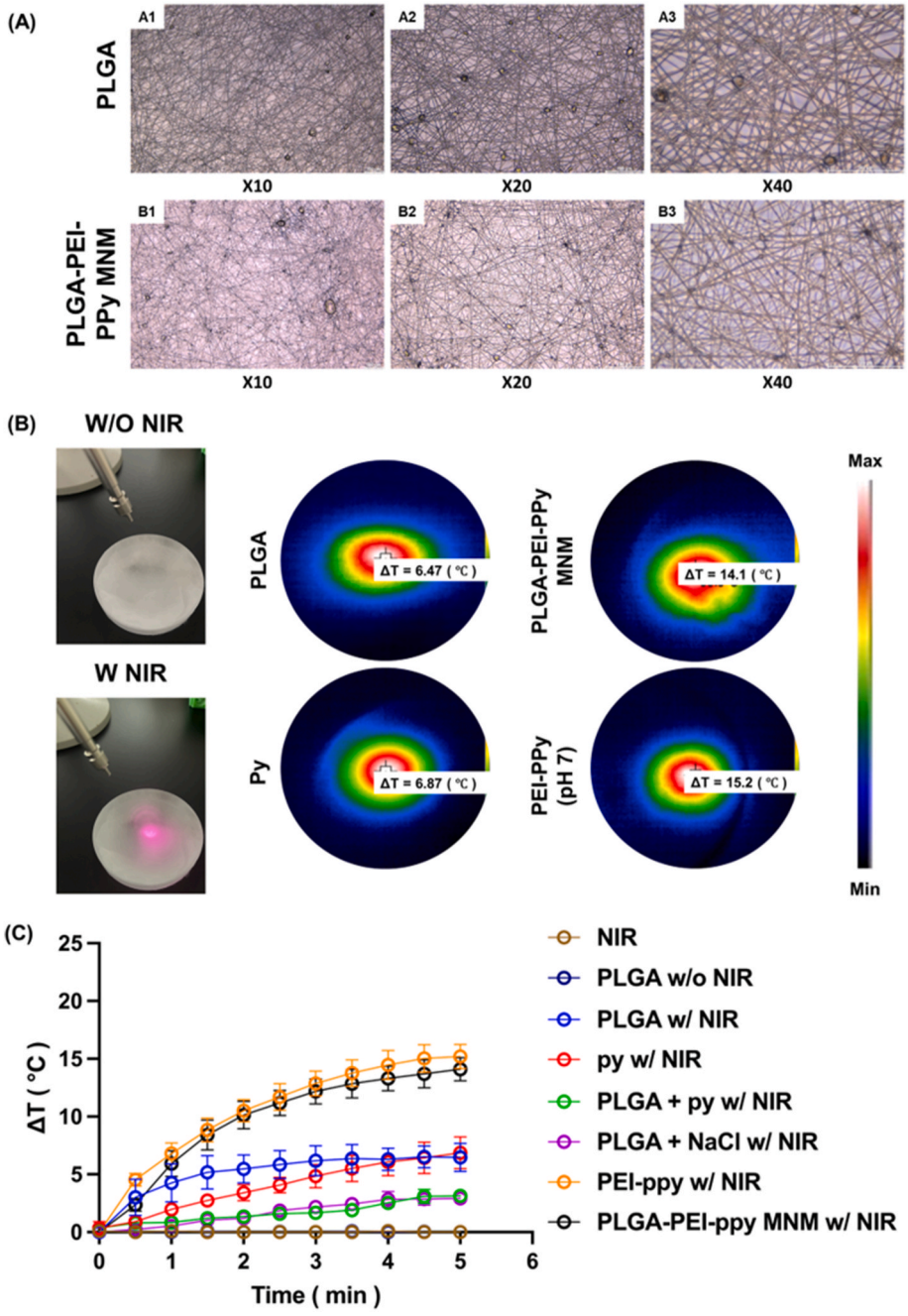

Fig. 3. Morphological structure and NIR-triggered photothermal behavior of electrospun membranes. (A) Bright-field microscopy images of pristine PLGA (A1–A3) and PLGA–PEI–PPy MNM (B1–B3) at increasing magnifications show fiber alignment, density, and particulate distribution.
(B) Photothermal performance under 808 nm NIR irradiation: visual, thermal, and (C) quantitative data confirm higher surface temperature elevation and photothermal conversion efficiency in PLGA–PEI–PPy MNM compared to PLGA, PEI, and pyrrole controls.

summary, the incorporation of polypyrrole and polyethyleneimine into the PLGA matrix alters the microstructural and thermal behavior of the electrospun membrane. The visible light microscopy data validate the compositional integration at the fiber level, while infrared thermographic analysis confirms the superior light-to-heat conversion efficiency of the PLGA-PEI-PPy MNM. These results underscore the potential of this multifunctional membrane as a wearable photothermal scaffold capable of achieving targeted therapeutic heating for clinical wound care applications.

To support the rationale of synergistic behaviour, we refer to the recent study by, which reported the development of a crosslinked polyimide-polypyrrole (4-POPPI-PPy) hybrid system demonstrating both high electrical conductivity (15.82 S/cm) and excellent thermal stability (Td_5 % = 431 °C). Notably, the authors emphasized that the integration of conjugated polypyrrole networks with thermally robust polymer backbones led to superior high-temperature conductivity retention and mechanical integrity, even after thermal annealing. This work illustrates how covalent integration of conductive and thermally active components can produce materials with synergistic functionalities a concept we aimed to replicate within our electrospun wound dressing system [26].

Finite element simulations of near-infrared (NIR) light penetration through wound dressings and skin can provide valuable insights into therapeutic depth, supporting the selection of the 808 nm wavelength

and corresponding irradiation settings. These simulations enable the optimization of treatment conditions by modeling light-tissue and light-material interactions, ensuring that sufficient energy reaches the targeted tissue layers for effective therapeutic outcomes. The 808 nm NIR wavelength is widely favored in photobiomodulation (PBM) therapy because of its superior tissue penetration compared to shorter wavelengths [27,28].

2.11. Cytocompatibility assessment of PEI-PPy complex and electrospun PLGA-PEI-PPy MNM

To evaluate the biocompatibility of the synthesized materials, a colorimetric MTT assay was conducted on L929 fibroblasts following treatment with serial dilutions of PEI-PPy complexes and electrospun PLGA-PEI-PPy micro/nanofibre membranes (PLGA-PEI-PPy MNM). The results, shown in Fig. 4, reflect cell metabolic activity in response to each formulation, with viability measured after 24 h of exposure to extract concentrations ranging 50 %–1 %.

As depicted in Fig. 4A, undiluted PEI-PPy extract (50 %) exhibited a pronounced cytotoxic effect, reducing cell viability to below 60 %, which is consistent with the known membrane-disruptive potential of branched PEI at high concentrations. However, upon serial dilution from 30 % to 1 %, a clear dose-dependent recovery in cell viability was observed. At the 10 % concentration, viability improved to approximately 90 %, comparable to control levels. This suggests that while PEI-PPy complexes can elicit cytotoxicity in high local concentrations, their biological compatibility can be readily modulated via dilution or encapsulation strategies.

In contrast, the electrospun PLGA-PEI-PPy MNM (Fig. 4B) demonstrated markedly improved cytocompatibility across all tested concentrations. At 50 % extract concentration, L929 viability remained above 50 %, indicating a reduction in cytotoxic potential compared to the PEI-PPy complex. At 30 %–1 % dilutions, viability values approached or exceeded about 90 %, further supporting the biocompatible nature of the membrane formulation. These results suggest that embedding PEI-PPy within the PLGA matrix via electrospinning likely provides a protective barrier, controlling the release of potentially toxic components and attenuating direct cell-membrane interactions.

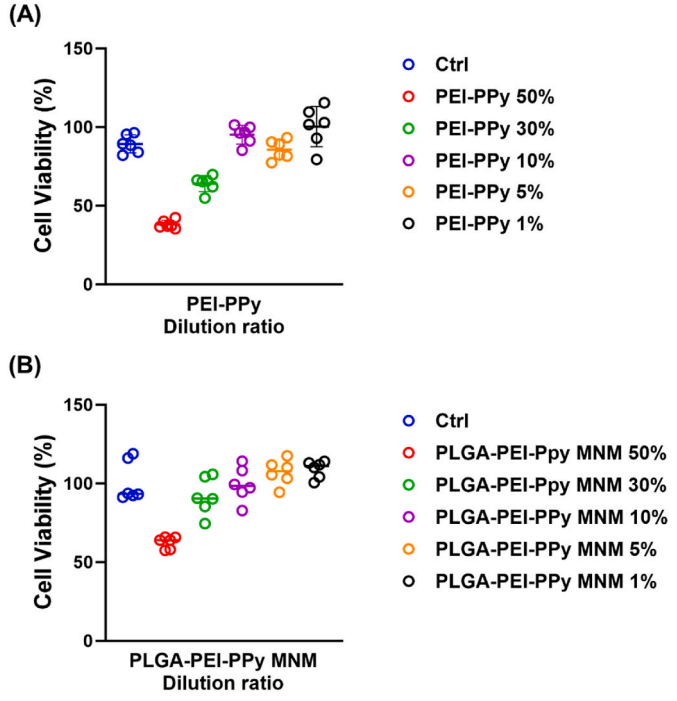

Fig. 4. Cytocompatibility evaluation of PEI-PPy complexes and PLGA-PEI-PPy MNM extracts using MTT assay. (A) L929 fibroblast viability after 24 h exposure to PEI–PPy extracts shows dose-dependent cytotoxicity, with reduction at 50 % and recovery at lower concentrations. (B) MTT assay of PLGA–PEI–PPy MNM extracts demonstrates enhanced cytocompatibility, with >90 % viability at most dilutions, indicating reduced toxicity through encapsulation within the PLGA matrix (mean ± SD).

The group-wise comparison underscores the functional advantage of structural integration: while PEI-PPy alone presents potential cytotoxicity at higher doses, the PLGA-PEI-PPy MNM formulation not only preserves the electroactive functionality of PPy but also mitigates adverse biological effects. This is particularly relevant for in vivo applications such as diabetic wound healing, where sustained cell viability in the wound bed is critical for tissue regeneration.

Collectively, these findings confirm that the PLGA-PEI-PPy MNM possesses excellent cytocompatibility, even at full-strength extract concentrations, and can serve as a safe platform for subsequent therapeutic use. The data also validate the efficacy of electrospinning as a strategy to stabilize and bio-shield reactive polymers, thereby bridging functionality and safety in advanced biomedical scaffolds.

2.12. In vivo evaluation of PLGA-PEI-PPy MNM for diabetic wound healing under NIR photothermal stimulation

To validate the therapeutic efficacy of the developed electrospun PLGA-PEI-PPy MNM, a streptozotocin (STZ)-induced diabetic wound model was established in Wistar rats, and the healing process was evaluated under controlled near-infrared (808 nm) stimulation. Fig. 5 summarizes the procedural steps, thermal responses, and biological outcomes associated with the experimental protocol.

As illustrated in Fig. 5A, the animal study commenced with STZ injection to induce hyperglycemia, followed by the creation of full-thickness dorsal wounds using a biopsy punch. The membranes were topically applied and irradiated using an 808 nm NIR light source in a non-contact configuration. All animals received sample administration + consistent photothermal treatment (5 min/day) under isoflurane anesthesia, ensuring reproducible exposure and minimal motion artifacts during NIR activation.

Wound photographs taken at serial timepoints (Fig. 5B) visually depict the progression of healing across different treatment arms. To further clarify spatial and temporal healing dynamics, wound margins were analyzed using ImageJ-based area tracking. Time-overlaid images demonstrate that wounds in the PLGA-PEI-PPy MNM + NIR group contracted more centrally and symmetrically over time, indicative of accelerated fibroblast migration and extracellular matrix remodeling. Notably, the wound bed in this group appeared cleaner and more vascularized, lacking necrotic crusts often seen in non-treated diabetic wounds, which are hallmarks of prolonged inflammation and poor perfusion.

These observations were supported by the wound closure quantification (Fig. 5C), which showed a statistically increase in closure rate in the PLGA-PEI-PPy MNM -treated group in wound area by day 7. In contrast, the untreated and PLGA-only groups achieved moderated closure rates, reflecting the limitations of passive wound coverage without photothermal or conductive augmentation. These cumulative results strongly support the hypothesis that PLGA-PEI-PPy MNM, when activated by NIR light, generates a biologically favorable microenvironment conducive to healing. The localized, mild hyperthermia not only enhances tissue perfusion but may also promote the expression of heat-shock proteins and reduce inflammatory cytokine load. Furthermore, the conductive nature of PPy may synergize with endogenous bioelectrical cues, facilitating cell migration and tissue integration—mechanisms that are particularly beneficial in diabetic wound beds characterized by chronic inflammation and impaired angiogenesis. Temperature measurements obtained via infrared thermography (Fig. 5D) revealed a distinct photothermal signature in animals treated with the PLGA-PEI-PPy MNM. Upon 808 nm irradiation, local skin

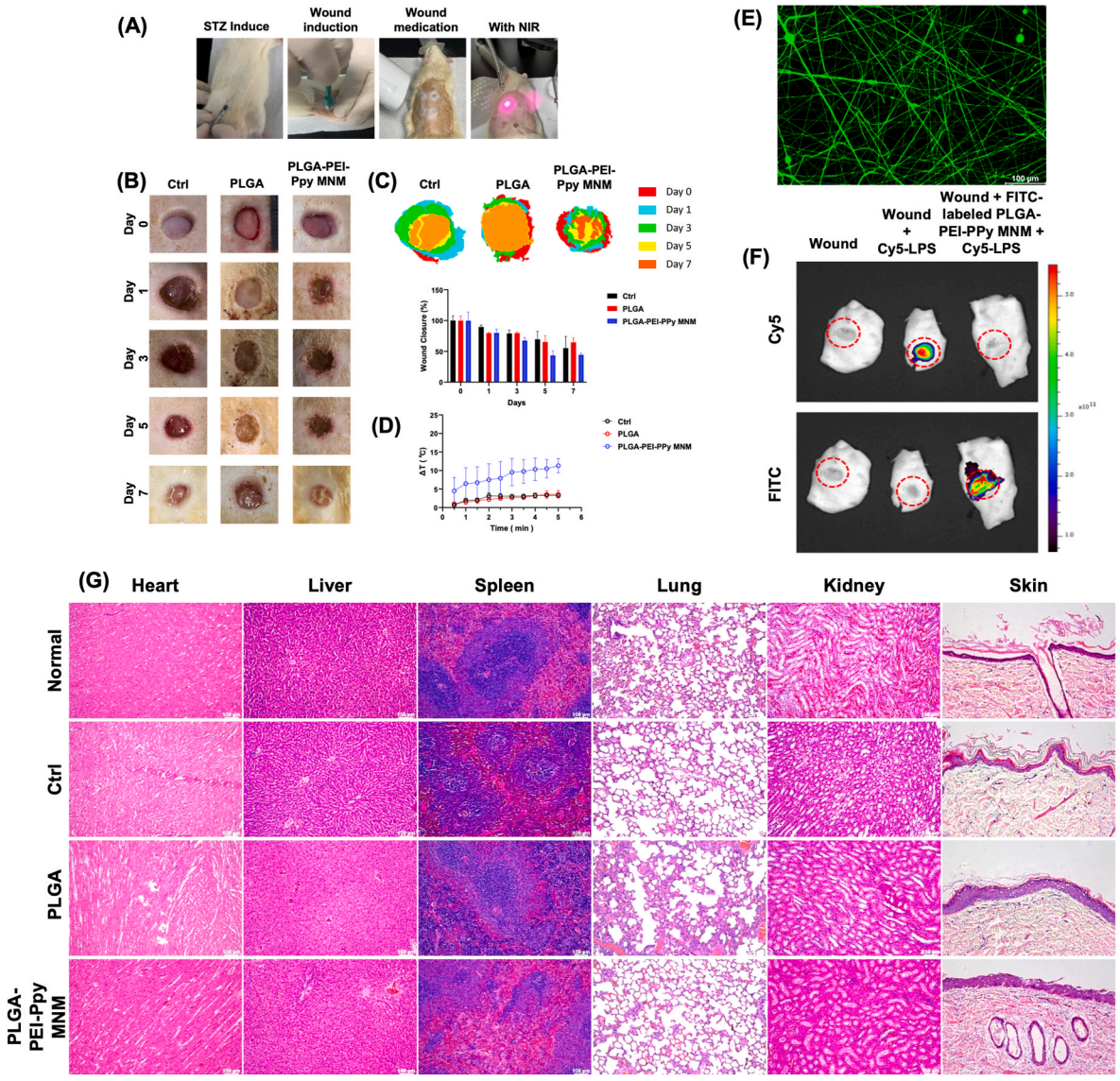

Fig. 5. In vivo evaluation of PLGA-PEI-PPy MNM for diabetic wound healing under near-infrared (NIR) stimulation. (A) Diabetic wounds were induced in Wistar rats via intraperitoneal STZ injection, followed by dorsal skin wound creation using a biopsy punch. Electrospun membranes were applied topically and exposed to 808 nm NIR light (2 W/cm^2, 5 min/day) under isoflurane anesthesia. (B) Time-lapse overlay maps over 7 days revealed centralized wound contraction in the PLGA-PEI-PPy MNM + NIR group, indicating enhanced tissue remodeling. (C) ImageJ-based quantification confirmed wound closure by day 7 in the PLGA-PEI-PPy MNM + NIR group, higher than controls. (D) Infrared thermal imaging showed that the PLGA–PEI–PPy MNM group reached mild hyperthermia (~43–45 °C, ΔT ~10–12 °C), while control and PLGA groups had minimal heating (ΔT < 4 °C). (E) Fluorescence microscopy of FITC-labeled PLGA–PEI–PPy MNM showed a dense, well-aligned fibrous network with uniform signal and suitable porosity. (F) In vivo IVIS imaging showed strong Cy5-LPS accumulation in untreated wounds, while PLGA-PEI-PPy MNM -pretreated wounds showed reduced fluorescence, demonstrating the membrane's barrier effect against exogenous inflammatory agents. (G) Representative H&E-stained sections of heart, liver, spleen, lung, kidney, and skin tissues across four experimental groups: Normal, Disease Control, PLGA, and PLGA–PEI–PPy MNM. Each column represents one organ in the same order across rows. Progressive recovery of tissue architecture is observed, particularly in the PLGA–PEI–PPy MNM group.

temperatures in this group increased by approximately 10–12 °C above baseline, reaching a therapeutic threshold (~43–45 °C) within minutes. In contrast, control groups including untreated wounds and those treated with pristine PLGA membranes demonstrated minimal temperature elevations (ΔT < 4 °C), indicating poor light-to-heat conversion capacity. This finding aligns with the in vitro thermal profiling and confirms the photothermal responsiveness of the conductive PLGA-PEI-PPy MNM NM system in vivo. In conclusion, the in vivo data confirm that the PLGA-PEI-PPy MNM, activated by short-term NIR exposure, accelerates wound closure in diabetic animals. This system represents a clinically relevant, non-invasive, and biologically compatible strategy for overcoming the complex healing barriers associated with diabetic chronic wounds.

2.13. In vitro visualization and in vivo pathogen exclusion capacity of PLGA-PEI-PPy MNM

To evaluate the structural uniformity and potential for bio-barrier functionality of the fabricated electrospun PLGA-PEI-PPy MNM, both in vitro and in vivo imaging strategies were employed. Fig. 5 summarizes the fluorescent visualization of the membrane network and its ability to function as a protective wound interface capable of excluding exogenous inflammatory stimuli.

As shown in Fig. 5E, fluorescence microscopy imaging of FITC-labeled PLGA-PEI-PPy MNM revealed a homogeneously distributed and interconnected fiber network, with well-aligned micro/nanofibres and minimal aggregation. The fluorescent signal was strongly retained

along the length of the fibrous architecture, suggesting effective FITC conjugation and physical encapsulation throughout the scaffold. Notably, the network density appeared sufficient to form a semi-permeable physical barrier while maintaining porosity appropriate for oxygen and nutrient exchange. The consistent fluorescence across the scaffold also confirmed the successful fabrication of an optically traceable version of the therapeutic membrane, suitable for in vivo localization and tracking.

To assess whether the membrane could serve as a passive physical shield to block pathogen infiltration in vivo, a comparative IVIS imaging experiment was conducted using Cy5-labeled lipopolysaccharide (Cy5-LPS) as a model inflammatory agent (Fig. 5F). Three groups were established: skin wounds alone, wounds exposed to Cy5-LPS, and wounds covered with FITC-PLGA-PEI-PPy MNM prior to Cy5-LPS administration. IVIS fluorescence data revealed strong Cy5 signals localized at the wound sites in the Cy5-LPS group, indicating successful delivery and penetration of the inflammatory pathogenic substance trigger into the exposed tissue. In sharp contrast, rats treated with PLGA-PEI-PPy MNM prior to Cy5-LPS exposure showed reduced Cy5 signal intensity at the wound area. This reduction indicates that the applied membrane effectively hindered LPS diffusion, likely acting as both a physical and electrostatic repellent barrier to macromolecular infiltration.

Interestingly, signal attenuation persisted even after spontaneous membrane detachment, suggesting the PLGA-PEI-PPy MNM had already modulated the local microenvironment either by sealing the wound bed or promoting early epithelial barrier restoration thereby diminishing subsequent inflammatory pathogenic substance diffusion. These findings hint at the membrane's dual capacity: not only does it function as a NIR-responsive photothermal scaffold but also as an intelligent barrier to external insults. This is particularly valuable in diabetic wounds, where heightened susceptibility to bacterial infection and impaired immune response render pathogen exclusion a critical factor in therapeutic success. Together, these in vitro and in vivo findings support the feasibility of the PLGA-PEI-PPy MNM as a multifunctional dressing that provides physical protection, optical traceability, and inflammation control. The integration of imaging functionality via FITC labeling further enables real-time membrane tracking and therapeutic monitoring, offering translational advantages for future clinical deployment.

Histopathological examination using H&E staining was performed on heart, liver, spleen, lung, kidney, and skin tissues collected from four groups: Normal, Control (disease model), PLGA-treated, and PLGA–PEI–PPy MNM-treated. In the HE test, all organs displayed intact and well-organized tissue architecture, with no signs of inflammation or structural damage (Fig. 5G).

Immunofluorescence staining was conducted to assess oxidative stress, angiogenesis, and inflammatory responses in skin wound tissues of diabetic rats across four groups: Normal, Control (diabetic wound untreated), PLGA-treated, and PLGA–PEI–PPy MNM-treated. Inflammatory activity was evaluated using IL-6 staining (green fluorescence), a key pro-inflammatory cytokine elevated in chronic wounds (Fig. 6A and C). The Control group demonstrated strong IL-6 expression, particularly in the epidermal and dermal layers surrounding the wound, indicative of ongoing inflammation. The PLGA group showed moderate IL-6 signal reduction, while the PLGA–PEI–PPy MNM group exhibited a substantial decrease in IL-6 expression, approaching the minimal levels observed in the Normal group. Quantitative analysis confirmed this trend, indicating that the PLGA-PEI-PPy MNM treatment effectively suppressed local inflammatory signaling.

To evaluate reactive oxygen species (ROS) accumulation at the wound site, tissue sections were stained with Amplex Red (red fluorescence), a well-established ROS indicator (Fig. 6B and C). The Control group exhibited strong Amplex Red signal throughout the wound bed, indicating high oxidative stress levels typical of diabetic wounds. In contrast, the PLGA-treated group showed a modest reduction in red fluorescence, while the PLGA–PEI–PPy MNM group displayed minimal fluorescence, suggesting a significant reduction in ROS levels along with normal group. This visual trend was confirmed by quantitative analysis, which showed that ROS levels were highest in the Control group and progressively lower in the PLGA and PLGA-PEI-PPy MNM groups, with the PLGA-PEI-PPy MNM group achieving nearly basal levels of oxidative stress comparable to normal tissue. Tumor Necrosis Factor-alpha (TNF-α) staining (green), a pro-inflammatory cytokine, showed intense fluorescence in the Control group, consistent with chronic inflammation in diabetic wounds. The PLGA group exhibited a moderate decrease in TNF-α expression, whereas the PLGA-PEI-PPy MNM -treated group demonstrated substantially lower TNF-α levels, approaching those seen in the Normal group. Quantification supported this observation, indicating effective suppression of inflammatory signalling by the PLGA–PEI–PPy MNM treatment (Fig. 6B and C).

To assess neovascularization, sections were stained for CD31 (green fluorescence), an endothelial marker specific for newly forming blood vessels tendency (Fig. 7A and C). The Normal group showed baseline vascular structures, while the Control group exhibited poor CD31 signal, indicating impaired angiogenesis in the diabetic wound environment. The PLGA group displayed a slight improvement, with localized CD31 expression near the wound edges. Notably, the PLGA–PEI–PPy MNM group exhibited a marked increase in CD31-positive signal distributed across the wound bed, signifying robust blood vessel formation. Quantification supported this observation, with the PLGA-PEI-PPy MNM group showing significantly enhanced angiogenic activity compared to all other groups.

Immunofluorescence staining was performed to evaluate cellular stress responses, inflammatory cytokine levels, and pro-angiogenic signalling in diabetic wound tissues following different treatments. Heat Shock Protein (HSP) staining (green fluorescence) revealed low expression in both the Normal and Control groups, with a slight increase in the PLGA group. Notably, the PLGA-PEI-PPy MNM group exhibited the strongest HSP signal, indicating enhanced cellular stress adaptation or protective response, likely induced by mild photothermal stimulation. Quantitative analysis confirmed significantly elevated HSP expression in the PLGA–PEI–PPy MNM group compared to all other groups (Fig. 7B and C). Vascular Endothelial Growth Factor (VEGF) staining (red fluorescence), a key regulator of angiogenesis, showed weak or absent expression in Normal, Control, and PLGA groups. In contrast, the PLGA–PEI–PPy MNM group displayed a robust and widespread VEGF signal throughout the wound area. This was confirmed by quantification, with the PLGA–PEI–PPy MNM group showing significantly higher VEGF expression, suggesting active promotion of angiogenic pathways essential for tissue regeneration (Fig. 7B and C).

3. Discussion

This study presents a novel multifunctional electrospun membrane that integrates photothermal conversion, electrical conductivity, and bio-barrier functionality, collectively addressing the complex pathophysiological challenges inherent in diabetic wound healing. By incorporating sodium chloride–templated PPy and PEI within a PLGA matrix, the resulting PLGA-PEI-PPy MNM via electrum spinning effectively converts near-infrared (NIR) light into localized heat. Our empirical evidence demonstrated that under 808 nm irradiation, the membrane rapidly achieves mild hyperthermia (43–45 °C) within minutes a temperature range known to upregulate heat shock proteins and reduce ROS without inflicting thermal damage. These observations are in line with recent studies that have highlighted the therapeutic potential of mild hyperthermia in modulating cellular stress responses and promoting tissue repair [29–31].

Recent advancements (2022–2025) have highlighted the growing potential of photothermal nanozyme-based platforms in addressing the dual challenge of bacterial infection and delayed healing in diabetic wounds. For instance, gold nanocluster-modified zirconium porphyrin MOFs (Au NCs@PCN) demonstrated potent ROS generation and

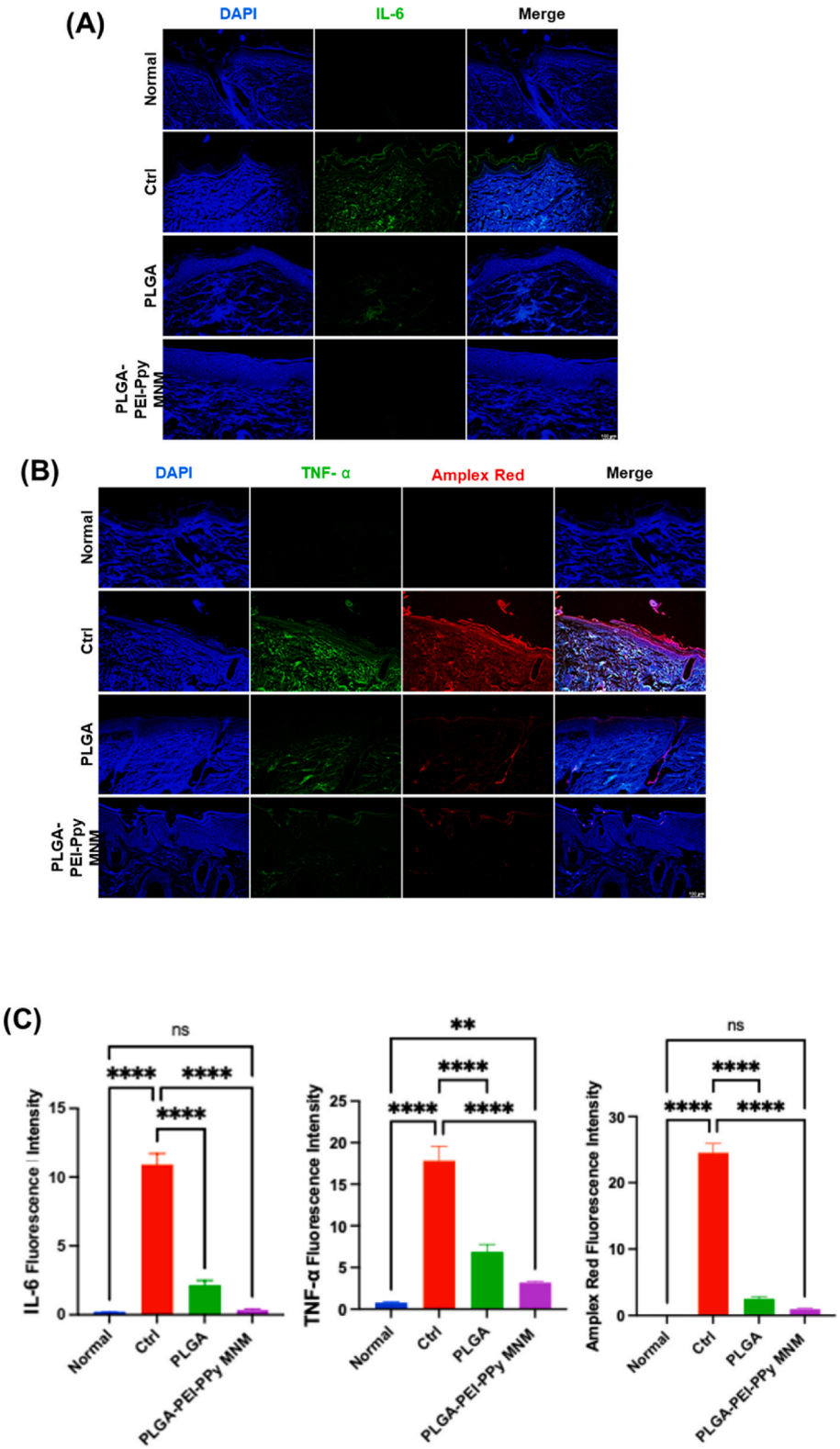

Fig. 6. Immunofluorescence analysis of oxidative stress, angiogenesis, and inflammation in diabetic wound tissues across treatment groups. (A) IL-6 staining reveals high inflammation in the Control group, moderately reduced in PLGA, and decreased in the PLGA-PEI-PPy MNM group. (B) TNF-α staining (green) reveals high inflammatory cytokine levels in the Control group, moderately reduced in PLGA, and suppressed in the PLGA-PEI-PPy MNM group. Amplex Red staining shows elevated ROS levels in the Control group, which are markedly reduced in PLGA and further suppressed in PLGA–PEI–PPy MNM-treated tissues. (C) Quantitative graphs on the right confirm statistical differences across groups. (For interpretation of the references to color in this figure legend, the reader is referred to the Web version of this article.)

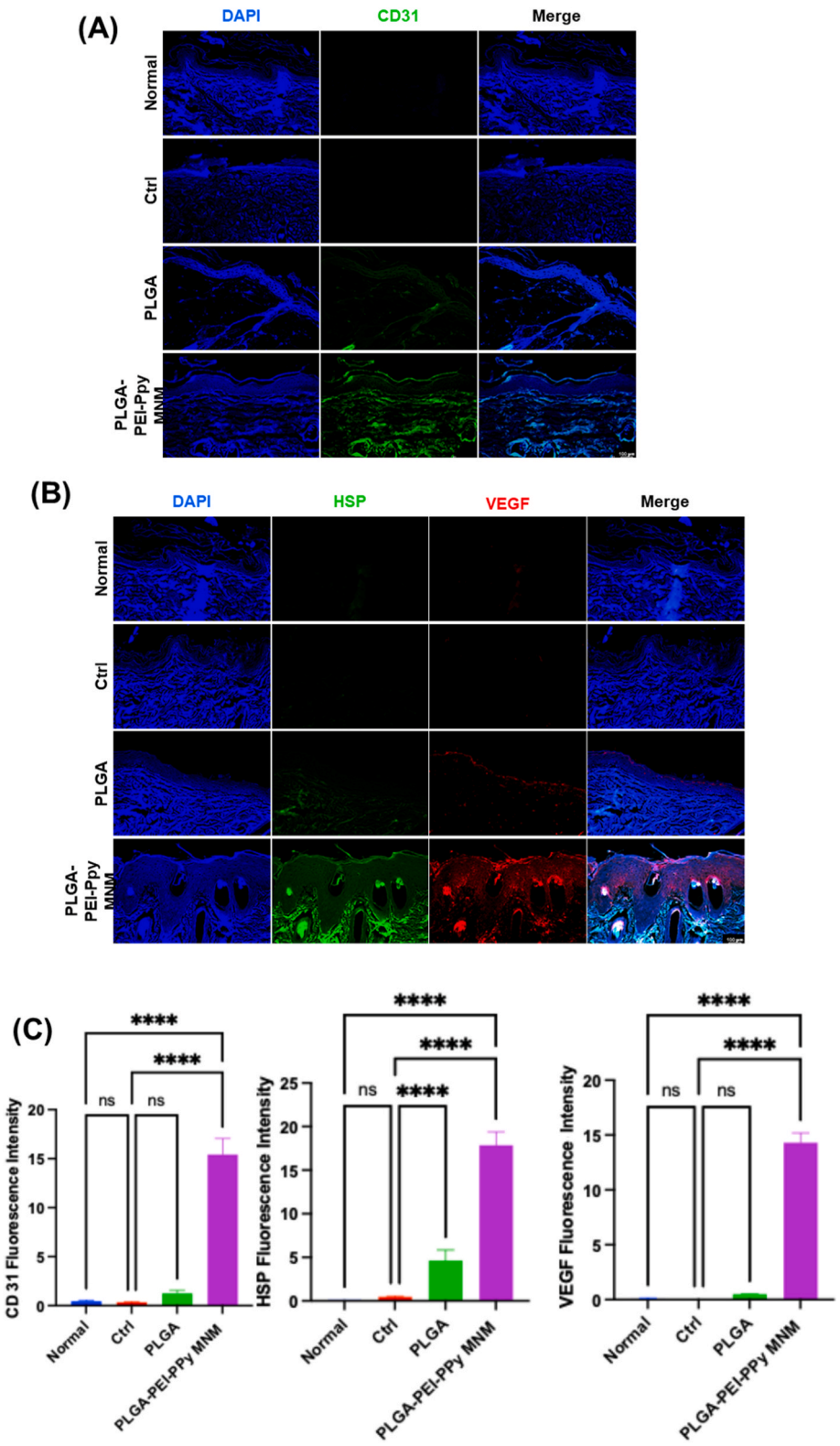

Fig. 7. Immunofluorescence analysis of cellular stress, inflammation, and angiogenesis in diabetic wound tissues following treatment. (A) CD31 staining indicates enhanced neovascularization in the PLGA-PEI-PPy MNM group compared to minimal expression in Control and PLGA groups. (B) HSP staining (green) shows elevated expression in the PLGA–PEI–PPy MNM group, indicating enhanced cellular stress adaptation compared to Normal, Control, and PLGA groups. VEGF staining (red) demonstrates minimal expression in Control and PLGA groups, with robust upregulation in the PLGA-PEI-PPy MNM -treated group, indicating strong pro-angiogenic signaling. DAPI (blue) stains nuclei in all panels. (C) Quantitative graphs at right confirm statistically significant differences across groups. (For interpretation of the references to color in this figure legend, the reader is referred to the Web version of this article.)

photothermal heating under NIR exposure, achieving >90 % bacterial inhibition and accelerating wound closure in diabetic rats [32]. Similarly, Ag-Hes nanoparticles (Ag-Hes NPs) embedded in hydrogel fibers via electrospinning showed strong antibacterial and anti-inflammatory activity by modulating IL-6, MMP9, and TNF-α levels, promoting collagen deposition and endothelial cell migration [33]. Another study reported the development of injectable, stretchable GelMA-Ag @Ti3C2-functionalized PVA/alginate hydrogels, which combined high porosity, NIR-responsive photothermal conversion, and ROS release to eliminateMRSA and E. coli, while also enhancing angiogenesis-related gene expression [34,35]. Additionally, Au-cluster-decorated Prussian blue nanozymes (PB-Au) exhibited tunable peroxidase-like activity and achieved ~95 % bacterial elimination and ~98 % wound closure by stimulating VEGF/CD31 expression and localized hyperthermia (~52 °C) [36].

Compared to these state-of-the-art NIR-responsive systems, our electrospun PLGA–PEI–PPy MNM introduces a unique combination of biocompatibility, reusability, breathability, and photothermal responsiveness, suitable for both wound dressing and wearable textile applications. Unlike injectable or hydrogel-based systems, our dry, flexible membrane supports non-invasive application and is capable of long-term structural stability under repeated NIR exposure, as demonstrated by retained thermal conversion and mechanical properties after washing and storage. Furthermore, the inclusion of cationic PEI not only enhances PPy dispersion but also modulates surface charge for bacterial capture and immune regulation, offering a multifunctional approach that goes beyond photothermal ablation alone. This work thus expands the application scope of NIR-responsive platforms to address both therapeutic and practical limitations associated with current electrospun nanomaterials.

Several NIR-responsive biomaterials have been explored for their antimicrobial and wound-healing properties. For example, Acticoat™, a commercially available silver-based dressing, exhibits broad-spectrum antimicrobial activity and rapid bactericidal effects through silver ion release. However, it lacks photothermal responsiveness and is not designed for reuse, raising concerns about cytotoxicity and environmental accumulation [37]. Similarly, graphene oxide-based materials have shown promising NIR photothermal conversion efficiency and antibacterial properties but are often limited by challenges in biocompatibility, dispersion stability, and integration into flexible, breathable substrates [38]. We would like to highlight that our group has previously reported a published study on NPP NPs–PEFM, a nanobased PEI–polypyrrole-coated polyethylene fiber membrane demonstrating excellent NIR photothermal conversion, biocompatibility, reusability, and effective antimicrobial activity. The fabric was also shown to provide warmth and reduce cold-induced vasoconstriction, highlighting its multifunctionality. This previous work provides a strong foundation for the development of advanced photothermal-responsive materials with potential applications in wearable protective fabrics and wound care, and it aligns with the approach taken in the present study [39]. The incorporation of PEI played a key role in stabilizing the PPy coating and enhancing the biological performance of the nanocomposite. Its strong positive surface charge not only promoted uniform nanoparticle attachment to the fabric but also facilitated electrostatic interactions with negatively charged bacterial membranes, contributing to effective bacterial capture and clearance. Although direct cell surface interaction analysis was not performed, the observed antibacterial efficacy and maintained cytocompatibility support PEI's dual role in structural stability and surface bioactivity modulation [39].

Both PLGA and PPy exhibit antimicrobial properties through different mechanisms. PLGA, a biodegradable and biocompatible polymer, is commonly utilized in drug delivery systems to prevent or eliminate microbial biofilms. It can inhibit biofilm formation and even disrupt existing biofilms when loaded with antimicrobial agents. Additionally, PLGA nanoparticles can release antibiotics in a controlled manner for sustained antibacterial action, while its biocompatibility and biodegradability make it ideal for encapsulating and delivering antimicrobial agents. The release of degradation products like lactic and glycolic acid also contributes to its antimicrobial effect [40–42]. In contrast, PPy, a conductive polymer, disrupts bacterial activity by interacting with bacterial cell membranes. Its positive charge enables it to bind to negatively charged bacterial membranes, potentially causing disruption and bacterial cell death. PPy is also used in composite materials with other antimicrobial agents, such as silver nanoparticles, to enhance its properties [43–46]. In summary, PLGA serves as an effective vehicle for delivering antimicrobial agents, while PPy directly interferes with bacterial membranes to exert its antimicrobial action.

In vitro experiments further underscore the promising cytocompatibility of the membrane. The encapsulation of PEI-PPy within the electrospun PLGA matrix ameliorated the cytotoxicity associated with high concentrations of PEI-PPy complexes when applied alone. L929 fibroblast viability improved markedly upon dilution and was further enhanced by the protective encapsulation provided by the PLGA scaffold. These findings support the concept that strategic polymer blending can stabilize reactive compounds and enhance the safety profile of advanced biomaterials, a concept that has been increasingly validated in recent literature on nanofiber-based wound dressings [47–51].

Importantly, the thermal behavior of the membrane is not solely a function of its photothermal conversion efficiency but is also intricately linked to the thermal-induced crosslinking of PPy within the composite. Thermal treatment during or post-electrospinning facilitates the formation of crosslinked networks in PPy, thereby enhancing its structural integrity and conductive pathways. This thermal-induced crosslinking minimizes polymer chain mobility and improves the mechanical stability of the fibers under repeated on/off irradiation cycles. Several studies have demonstrated that moderate thermal processing can induce interchain crosslinking in conductive polymers like PPy, leading to enhanced electrical conductivity and durability in bioelectronic applications [52,53]. In our system, the thermal polymerization at 80 °C in the presence of NaCl likely promoted partial crosslinking of PPy, which not only stabilized the conductive network but also contributed to the homogeneous photothermal field observed during NIR exposure. This crosslinked architecture is critical for ensuring consistent heat generation and minimizes potential leaching of reactive species, thereby supporting both the photothermal and biological performance of the PLGA-PEI-PPy MNM.

The in vivo studies using a streptozotocin-induced diabetic rat model further revealed that the PLGA-PEI-PPy MNM, when activated by short-term daily NIR irradiation, accelerated wound closure compared to both untreated controls and PLGA-only dressings. Enhanced wound healing was supported by rapid tissue contraction, improved neovascularization, and reduced inflammatory infiltrates [54]. The photothermal stimulation appears to enhance local blood flow and promote the expression of beneficial cytokines and growth factors, thereby facilitating a more robust tissue regeneration response. Moreover, the additional barrier function provided by the membrane, as demonstrated by the reduced diffusion of Cy5-labeled lipopolysaccharide (LPS) in IVIS imaging, suggests that this platform not only promotes healing through thermal and conductive cues but also protects the wound from exogenous pathogens. These multifaceted benefits align with recent advancements in smart wound dressings that combine therapeutic and diagnostic capabilities for improved clinical outcomes [15,55].

The integration of imaging functionalities via FITC labeling for in vitro tracking and the use of Cy5-LPS for in vivo inflammatory assessment further enhances the translational potential of our design. Real-time monitoring of the membrane's integrity and its protective function against pathogenic infiltration provides critical feedback, enabling fine-tuning of treatment protocols. In diabetic wounds, where the risk of infection is compounded by impaired immune responses, such smart dressings offer a clinical advantage [56].

Overall, the findings of this study underscore the translational promise of the PLGA-PEI-PPy MNM as an intelligent, light-responsive

dressing capable of overcoming the multifactorial barriers to diabetic wound healing. The synergistic combination of photothermal, conductive, and barrier properties not only accelerates tissue repair but also offers non-invasive protection of the wound microenvironment. Future investigations should explore long-term biocompatibility, potential for controlled drug release, and further optimization of thermal-induced crosslinking parameters to maximize both mechanical stability and therapeutic efficacy. Continued research in this direction will pave the way for next-generation intelligent bandages that substantially improve patient outcomes in diabetic wound management.

4. Conclusion

This study presents a multifunctional, electrospun micro/nanofibre membrane (PLGA-PEI-PPy MNM) that combines conductive, photothermal, and barrier functionalities to address the complex pathophysiology of diabetic chronic wounds. By integrating sodium chloride–templated PLGA-PEI-PPy MNM under thermal process into a conformal, sprayable scaffold, we successfully engineered a wearable dressing capable of wireless NIR-responsive heating, pathogen exclusion, and cellular support.

Comprehensive physicochemical characterization confirmed the redox activity, colloidal stability, hydrophilic modulation, and compositional uniformity of the PLGA-PEI-PPy MNM. The membrane exhibited rapid and reproducible photothermal conversion under 808 nm NIR irradiation, achieving therapeutic temperatures (~45 °C) within minutes without thermal degradation. In vitro assays demonstrated cytocompatibility with L929 fibroblasts in a dose-dependent manner of tested samples.

In vivo, the PLGA-PEI-PPy MNM accelerated wound healing in a streptozotocin-induced diabetic rat model. Compared to untreated and PLGA-only controls, the PLGA-PEI-PPy MNM -treated group showed an enhanced wound closure, improved neovascularization, and reduced inflammatory infiltrates under daily short-duration NIR exposure. Moreover, IVIS fluorescence imaging confirmed the membrane's capacity to serve as a barrier against foreign pathogenic substance stimuli such as lipopolysaccharide (LPS), even after spontaneous detachment from the wound bed.

Taken together, these findings support the translational potential of the PLGA-PEI-PPy MNM as an intelligent, non-invasive, and patient-friendly wound dressing platform. Its lightweight, sprayable configuration, combined with photothermal controllability and bio-barrier properties, offers a compelling strategy to overcome the multifactorial healing deficits in diabetic wounds. Future work will focus on scaling this platform for clinical deployment and integrating biosensing or drug-release modules to further enhance therapeutic precision and wound monitoring.

CRediT authorship contribution statement

Chun-Chi Chang: Conceptualization, Data curation, Methodology, Writing – original draft, Writing – review & editing. **Ting-Chiau Huang:** Conceptualization, Data curation, Methodology, Writing – original draft, Writing – review & editing. **Jia-Wei Liang:** Data curation, Methodology, Formal analysis, Writing – original draft, Writing – review & editing. **Sih-Chi Chuang:** Data curation, Methodology, Formal analysis, Writing – original draft, Writing – review & editing. **Ching-Cheng Huang:** Writing – review & editing. **Hieu Trung Nguyen:** Writing – review & editing. **Hsien-Tsung Lu:** Conceptualization, Data curation, Methodology, Formal analysis, Funding acquisition, Investigation, Project administration, Resources, Supervision, Validation, Software, Visualization, Writing – original draft, Writing – review & editing. **Ke-Hung Tsui:** Conceptualization, Data curation, Methodology, Formal analysis, Funding acquisition, Investigation, Project administration, Resources, Supervision, Validation, Software, Visualization, Writing – original draft, Writing – review & editing. **Andrew E.-Y. Chuang:** Conceptualization, Data curation, Methodology, Formal analysis, Funding acquisition, Investigation, Project administration, Resources, Supervision, Validation, Software, Visualization, Writing – original draft, Writing – review & editing.

Consent for publication

All of the authors involved in this study have agreed to the publication of this manuscript.

Declaration of competing interest

All authors declare that no conflicts of interest exist.

Acknowledgments

This study was financially supported by grants from the National Science and Technology Council (NSTC), Taiwan [grant numbers 112-2221-E-038 -002 -MY3, and 113-2314-B-038-MY3]. The Taipei Medical University also supports this work (TMU111-AE1-B03).

Appendix A. Supplementary data

Supplementary data to this article can be found online at https://doi.org/10.1016/j.jddst.2025.107392.

Data availability

The data will be available on request.

References

[1] D.G. Armstrong, T.W. Tan, A.J.M. Boulton, S.A. Bus, Diabetic foot ulcers: a review, JAMA 330 (2023) 62–75.
[2] J.L. Burgess, W.A. Wyant, B. Abdo Abujamra, R.S. Kirsner, I. Jozic, Diabetic wound-healing science, Medicina (Kaunas) 57 (2021).
[3] J. Kim, The pathophysiology of diabetic foot: a narrative review, J. Yeungnam Med. Sci. 40 (2023) 328–334.
[4] N. Dasari, A. Jiang, A. Skochdopole, J. Chung, E.M. Reece, J. Vorstenbosch, S. Winocour, Updates in diabetic wound healing, inflammation, and scarring, Semin. Plast. Surg. 35 (2021) 153–158.
[5] L. Deng, C. Du, P. Song, T. Chen, S. Rui, D.G. Armstrong, W. Deng, The role of oxidative stress and antioxidants in diabetic wound healing, Oxid. Med. Cell. Longev. 2021 (2021) 8852759.
[6] O.O. Oguntibeju, Type 2 diabetes mellitus, oxidative stress and inflammation: examining the links, Int. J. Physiol. Pathophysiol. Pharmacol. 11 (2019) 45–63.
[7] Y. Cai, T. Chai, W. Nguyen, J. Liu, E. Xiao, X. Ran, Y. Ran, D. Du, W. Chen, X. Chen, Phototherapy in cancer treatment: strategies and challenges, Signal Transduct. Targeted Ther. 10 (2025) 115.
[8] G. Wei, G. Yang, Y. Wang, H. Jiang, Y. Fu, G. Yue, R. Ju, Phototherapy-based combination strategies for bacterial infection treatment, Theranostics 10 (2020) 12241–12262.
[9] Q. Yu, X. Tang, W. Zhao, Y. Qiu, J. He, D. Wan, J. Li, X. Wang, X. He, Y. Liu, M. Li, Z. Zhang, Q. He, Mild hyperthermia promotes immune checkpoint blockade-based immunotherapy against metastatic pancreatic cancer using size-adjustable nanoparticles, Acta Biomater. 133 (2021) 244–256.
[10] M. Payne, S.H. Bossmann, M.T. Basel, Direct treatment versus indirect: thermoablative and mild hyperthermia effects, Wiley Interdiscip. Rev. Nanomed. Nanobiotechnol. 12 (2020) e1638.
[11] Y. Chen, M. Shafiq, M. Liu, Y. Morsi, X. Mo, Advanced fabrication for electrospun three-dimensional nanofiber aerogels and scaffolds, Bioact. Mater. 5 (2020) 963–979.
[12] Z. Yu, H. Wang, B. Ying, X. Mei, D. Zeng, S. Liu, W. Qu, X. Pan, S. Pu, R. Li, Y. Qin, Mild photothermal therapy assist in promoting bone repair: related mechanism and materials, Mater. Today Bio 23 (2023) 100834.
[13] W. Lin, S. Sun, D. Zhang, Y. Liu, J. Yu, R. Liu, K. Wang, H. Kan, K. Dong, C. Xu, Near-infrared light-responsive nanofibrous membranes for treatment of bacterial wound infections, ACS Appl. Nano Mater. 6 (2023) 20298–20309.
[14] Q. Zheng, Y. Xi, Y. Weng, Functional electrospun nanofibers: fabrication, properties, and applications in wound-healing process, RSC Adv. 14 (2024) 3359–3378.
[15] J. Fu, D. Wang, Z. Tang, Y. Xu, J. Xie, R. Chen, P. Wang, Q. Zhong, Y. Ning, M. Lei, H. Mai, H. Li, H. Liu, J. Wang, H. Cheng, NIR-responsive electrospun nanofiber dressing promotes diabetic-infected wound healing with programmed combined temperature-coordinated photothermal therapy, J. Nanobiotechnol. 22 (2024) 384.

[16] N. Zhang, D.H. Kohn, Using polymeric materials to control stem cell behavior for tissue regeneration, Birth Defects Res. C Embryo Today Off. 96 (2012) 63–81.
[17] S. Tiwari, S. Namsani, J.K. Singh, Effect of salt on the adsorption of ionic surfactants at the air-water interface, J. Mol. Liq. 360 (2022).
[18] Q. Lei, D. He, L. Ding, F. Kong, P. He, J. Huang, J. Guo, C.J. Brinker, G. Luo, W. Zhu, Y. Yu, Microneedle patches integrated with biomineralized melanin nanoparticles for simultaneous skin tumor photothermal therapy and wound healing, Adv. Funct. Mater. 32 (2022) 2113269.
[19] T. Xiang, Q. Guo, L. Jia, T. Yin, W. Huang, X. Zhang, S. Zhou, Multifunctional hydrogels for the healing of diabetic wounds, Adv. Healthcare Mater. 13 (2024) e2301885.
[20] N. Xu, Y. Gao, Z. Li, Y. Chen, M. Liu, J. Jia, R. Zeng, G. Luo, J. Li, Y. Yu, Immunoregulatory hydrogel decorated with Tannic acid/Ferric ion accelerates diabetic wound healing via regulating Macrophage polarization, Chem. Eng. J. 466 (2023) 143173.
[21] F. Akhter, S. Manrique-Bedoya, C. Moreau, A.L. Smith, Y. Feng, K.M. Mayer, R. L. Hood, Assessment and modeling of plasmonic photothermal therapy delivered via a fiberoptic microneedle device Ex vivo, Pharmaceutics 13 (2021).
[22] D. Scieglinska, Z. Krawczyk, D.R. Sojka, A. Gogler-Piglowska, Heat shock proteins in the physiology and pathophysiology of epidermal keratinocytes, Cell Stress Chaperones 24 (2019) 1027–1044.
[23] Z. Chen, Q. Mo, D. Mo, X. Pei, A. Liang, J. Cai, B. Zhou, L. Zheng, H. Li, F. Yin, J. Zhao, A multifunctional photothermal electrospun PLGA/MoS(2)@Pd nanofiber membrane for diabetic wound healing, Regen. Biomater. 12 (2025) rbae143.
[24] J. Szyller, I. Bil-Lula, Heat shock proteins in oxidative stress and Ischemia/Reperfusion Injury and benefits from physical exercises: a review to the current knowledge, Oxid. Med. Cell. Longev. 2021 (2021) 6678457.
[25] C.O. Yu, K.S. Leung, K.P. Fung, F.F. Lam, E.S. Ng, K.M. Lau, S.K. Chow, W. H. Cheung, The characterization of a full-thickness excision open foot wound model in n5-streptozotocin (STZ)-induced type 2 diabetic rats that mimics diabetic foot ulcer in terms of reduced blood circulation, higher C-reactive protein, elevated inflammation, and reduced cell proliferation, Exp. Anim. 66 (2017) 259–269.
[26] P. He, J. Tan, J. Huang, P. Yu, J. Guo, Y. Chen, Y. Liu, Design, synthesis and properties of conductive crosslinked polyimide-polypyrrole with high thermal stability, Polymer 333 (2025) 128659.
[27] C. Ash, M. Dubec, K. Donne, T. Bashford, Effect of wavelength and beam width on penetration in light-tissue interaction using computational methods, Laser Med. Sci. 32 (2017).
[28] M.V. Padalkar, N. Pleshko, Wavelength-dependent penetration depth of near infrared radiation into cartilage, Analyst 140 (2015) 2093–2100.
[29] L. Mei, Y. Zhang, K. Wang, S. Chen, T. Song, Nanomaterials at the forefront of antimicrobial therapy by photodynamic and photothermal strategies, Mater. Today Bio 29 (2024) 101354.
[30] Y. Qu, K. Lu, Y. Zheng, C. Huang, G. Wang, Y. Zhang, Q. Yu, Photothermal scaffolds/surfaces for regulation of cell behaviors, Bioact. Mater. 8 (2022) 449–477.
[31] S. Chen, Y. Xie, K. Ma, Z. Wei, X. Ran, X. Fu, C. Zhang, C. Zhao, Electrospun nanofibrous membranes meet antibacterial nanomaterials: from preparation strategies to biomedical applications, Bioact. Mater. 42 (2024) 478–518.
[32] X. Zhao, L. Chang, Y. Hu, S. Xu, Z. Liang, X. Ren, X. Mei, Z. Chen, Preparation of photocatalytic and antibacterial MOF nanozyme used for infected diabetic wound healing, ACS Appl. Mater. Interfaces 14 (2022) 18194–18208.
[33] X. Ren, Y. Hu, L. Chang, S. Xu, X. Mei, Z. Chen, Electrospinning of antibacterial and anti-inflammatory Ag@hesperidin core-shell nanoparticles into nanofibers used for promoting infected wound healing, Regen Biomater 9 (2022 Feb 18) rbac012, https://doi.org/10.1093/rb/rbac012. PMID: 35592139; PMCID: PMC9113224.
[34] Z. Liang, Z. Sang, Y. Li, Z. Chen, X. Mei, X. Ren, Enhancing the performance of injectable self-activating PVA-alginate hydrogel by Ag@MXene nanozyme as NIR responsive and photoenhanced antibacterial platform for wound healing, Carbohydr. Polym. 357 (2025) 123434.
[35] F. Wang, Q. Sun, Y. Li, R. Xu, R. Li, D. Wu, R. Huang, Z. Yang, Y. Li, Hydrogel Encapsulating Wormwood Essential Oil with Broad-spectrum Antibacterial and Immunomodulatory Properties for Infected Diabetic Wound Healing, Adv Sci (Weinh) 11 (3) (2024 Jan) e2305078, https://doi.org/10.1002/advs.202305078. Epub 2023 Nov 29. PMID: 38030556; PMCID: PMC10797468.
[36] X. Ren, Y. Hu, L. Chang, S. Xu, X. Mei, Z. Chen, Electrospinning of antibacterial and anti-inflammatory Ag@hesperidin core-shell nanoparticles into nanofibers used for promoting infected wound healing, Regen. Biomater. 9 (2022).
[37] ACTICOAT*, Wound Antimicrobial Dressing | Nanocrystalline Silver, Woundsource, com, 2016.
[38] S. Hao, H. Han, Z. Yang, M. Chen, Y. Jiang, G. Lu, L. Dong, H. Wen, H. Li, J. Liu, L. Wu, Z. Wang, F. Wang, Recent advancements on photothermal conversion and antibacterial applications over MXenes-Based materials, Nano-Micro Lett. 14 (2022) 178.
[39] Y.-C. Hsiao, P.-R. Jheng, H.T. Nguyen, Y.-H. Chen, Y.B. Manga, L.-S. Lu, L. Rethi, C.-H. Chen, T.-W. Huang, J.-D. Lin, T.-K. Chang, Y.-C. Ho, E.-Y. Chuang, Photothermal-Irradiated polyethyleneimine–polypyrrole nanopigment film-coated polyethylene fabrics for infrared-inspired with pathogenic evaluation, ACS Appl. Mater. Interfaces 13 (2021) 2483–2495.
[40] A. Shariati, Z. Chegini, E. Ghaznavi-Rad, E.N. Zare, S.M. Hosseini, PLGA-based nanoplatforms in drug delivery for inhibition and destruction of microbial biofilm, Front. Cell. Infect. Microbiol. 12 (2022) 926363.
[41] Y. Cheng, J. Qin, Y. Huang, T. Wang, The antimicrobial effects of PLGA microspheres containing the antimicrobial peptide OP-145 on clinically isolated pathogens in bone infections, Sci. Rep. 12 (2022) 14541.
[42] A.K. Shakya, M. Al-Sulaibi, R.R. Naik, H. Nsairat, S. Suboh, A. Abulaila, Review on PLGA polymer based nanoparticles with antimicrobial properties and their application in various medical conditions or infections, Polymers 15 (2023).
[43] Y. Zhu, B. Chen, Y. Liu, T. Tan, B. Gao, L. Lu, P. Zhu, Y. Mao, Recent advances in conductive hydrogels for electronic skin and healthcare monitoring, Biosensors 15 (2025) 463.
[44] M. Moorthy, S. Arumugam, A. Gupta, J. Luong, A. Gedanken, Antimicrobial activities of conducting polymers and their composites, Macromol 2 (2022) 78–99.
[45] Y. Wu, Q. Ruan, C. Huang, Q. Liao, L. Liu, P. Liu, S. Mo, G. Wang, H. Wang, P. K. Chu, Balancing the biocompatibility and bacterial resistance of polypyrrole by optimized silver incorporation, Biomater. Adv. 134 (2022) 112701.
[46] M.H.R. Borges, B.E. Nagay, R.C. Costa, J.G.S. Souza, M.T. Mathew, V.A.R. Barão, Recent advances of polypyrrole conducting polymer film for biomedical application: toward a viable platform for cell-microbial interactions, Adv. Colloid Interface Sci. 314 (2023) 102860.
[47] B. Yan, Y. Hua, J. Wang, T. Shao, S. Wang, X. Gao, J. Gao, Surface modification progress for PLGA-based cell scaffolds, Polymers 16 (2024).
[48] Z. Jiang, Z. Zheng, S. Yu, Y. Gao, J. Ma, L. Huang, L. Yang, Nanofiber scaffolds as drug delivery systems promoting wound healing, Pharmaceutics 15 (2023).
[49] N. Palani, P. Vijayakumar, P. Monisha, S. Ayyadurai, S. Rajadesingu, Electrospun nanofibers synthesized from polymers incorporated with bioactive compounds for wound healing, J. Nanobiotechnol. 22 (2024) 211.
[50] P.D. Yadav, P.V. Londhe, S.S. Chavan, D.D. Mohite, G.B. Firame, S.S. Kadam, M. J. Patil, M.I. Ansari, Electrospun composite nanofibers for wound healing: synthesis, characterization, and clinical potential of biopolymer-based materials, Discov. Mater. 4 (2024).
[51] Y. Liu, C. Li, Z. Feng, B. Han, D.G. Yu, K. Wang, Advances in the preparation of nanofiber dressings by electrospinning for promoting diabetic wound healing, Biomolecules 12 (2022).
[52] C.R. Broda, J.Y. Lee, S. Sirivisoot, C.E. Schmidt, B.S. Harrison, A chemically polymerized electrically conducting composite of polypyrrole nanoparticles and polyurethane for tissue engineering, J. Biomed. Mater. Res. 98 (2011) 509–516.
[53] Y. Liang, J.C. Goh, Polypyrrole-incorporated conducting constructs for tissue engineering applications: a review, Bioelectricity 2 (2020) 101–119.
[54] M. Chen, F. Wang, Q. Yan, M. Da, F. Wang, Photothermally responsive graphene hybrid dry powders for diabetic wound healing, Biomed. Phys. Eng. Express 10 (2024).
[55] W. Zhang, L. Liu, H. Cheng, J. Zhu, X. Li, S. Ye, X. Li, Hydrogel-based dressings designed to facilitate wound healing, Mater. Adv. 5 (2024) 1364–1394.
[56] A. Schmidtchen, M. Puthia, Real-time in vivo imaging of LPS-induced local inflammation and drug deposition in NF-kappaB reporter mice, Bio. Protoc. 10 (2020) e3724.